Renewable and Sustainable Energy Reviews 29 (2014) 301–315

Contents lists available at ScienceDirect

Renewable and Sustainable Energy Reviews

journal homepage: www.elsevier.com/locate/rser

Review on the heat dissipation performance of battery pack with different structures and operation conditions

X.M. Xu*, R. He

School of Automotive and Traffic Engineering, Jiangsu University, Zhenjiang 212013, China

ARTICLE INFO

Article history:
Received 29 April 2013
Received in revised form
5 August 2013
Accepted 11 August 2013
Available online 20 September 2013

Keywords:
Battery pack
Operation condition
Thermal power
Heat dissipation performance
SOC state
Charge and discharge rate

ABSTRACT

This paper reviews the heat dissipation performance of battery pack with different structures (including: longitudinal battery pack, horizontal battery pack, and changing the position of air-inlet and air-outlet) and operation conditions (including: SOC state, charge and discharge rate, and practical operation condition), and finally arrives at the conclusions as follows: the average thermal power of 55 Ah lithium-ion battery monomer decreases along with environment temperature rising, SOC state decreasing and charge and discharge rate falling; the maximum temperature rising and temperature difference of battery pack are not only relevant to the flow rate, but also related to the airflow duct structure, the battery pack with air-inlets on both sides is more conducive to the forced air cooling; the flow rate of battery pack at 70% SOC state is maximum, the maximum temperature rising and temperature difference of battery pack at 70% SOC state are minimum, and that of 90% SOC state are maximum; the flow rate and the average pressure drop between air-inlet and air-outlet both decrease along with charge and discharge rate increasing, but the maximum temperature rising and temperature difference of battery pack increase; as considering the practical operation condition of battery pack, the charge and discharge rate is between 0.5 C and 0.8 C, and the maximum temperature rising and maximum temperature difference of battery pack are 7.61 °C and 4.29 °C. Then the reference basis for heat flow field characteristic analysis and structure design of battery pack are offered.

Contents

* Corresponding author. Tel.: +86 511 88780271; fax: +86 511 88780271 2009.
E-mail address: xuxiaoming3777@163.com (X.M. Xu).

1364-0321/$ - see front matter Crown Copyright © 2013 Published by Elsevier Ltd. All rights reserved.
http://dx.doi.org/10.1016/j.rser.2013.08.057

1. Introduction

Today the vehicle manufacturers are forced to shift their attention to green energy power and clean vehicles [1–8]. Pure electric vehicle (EV), hybrid electric vehicle (HEV) and fuel cell electric vehicle (FCEV) are more energy efficient and cleaner than conventional vehicle [9–17]. Battery pack is the power source of electric vehicle, and it generates much heat during rapid charge and discharge cycles at high current levels, such as during quick acceleration, with various chemical and electrochemical reactions [18–23]. Thus thermal behavior and heat transfer within the battery pack attract more attention [24–28], a well-designed cooling system is an essential part in the battery pack to safely maintain the battery temperature under the required conditions [29–32].

Cooling methods of battery pack including: air cooling [33–35], liquid cooling [36–38], and PCM cooling [39–41], and the air cooling divides into nature air cooling and forced air cooling. Considering the cost and space limitation, the forced air cooling is widely used as the cooling method of battery pack at home and abroad [42–44], many researchers have carried out the related work: for battery pack arrangement, Takaki [45] separated the forced air cooling into serial airflow and parallel airflow; the forced air cooling system developed by Toyota corporation was the most representative, and the relevant patents were applied [46]; Pan [47] researched the heat dissipation performance of Hybrid-Electric vehicle battery pack by software STAR-CD and ANSYS, and validated by experiments; Fu [48] researched the thermal management system of Ni-MH battery pack; Zhu [49] researched the thermal management system of electric vehicle battery pack, and analyzed the cooling system structure design of Toyota RAV-4 electric vehicle; when the speed of electric vehicle was constant, Liu [50] researched the temperature field of lithium-ion battery pack based on natural air cooling by simulation and experiment. In addition, there are many forced air cooling system of battery pack developed by researchers and manufacturers [51–53], in order to improve the temperature distribution uniformity of battery module.

The authors have taken some studies on cooling system design of electric vehicle, including: nature air cooling [54–58] (Fig. 1(a) shows the temperature field distribution of electric vehicle basing on the nature air cooling), forced air cooling [59] (Fig. 1(b) shows the temperature field distribution of battery pack basing on the forced air cooling), and liquid cooling [58,60] (Fig. 1(c) shows the liquid cooling system of battery module), and then contribute a

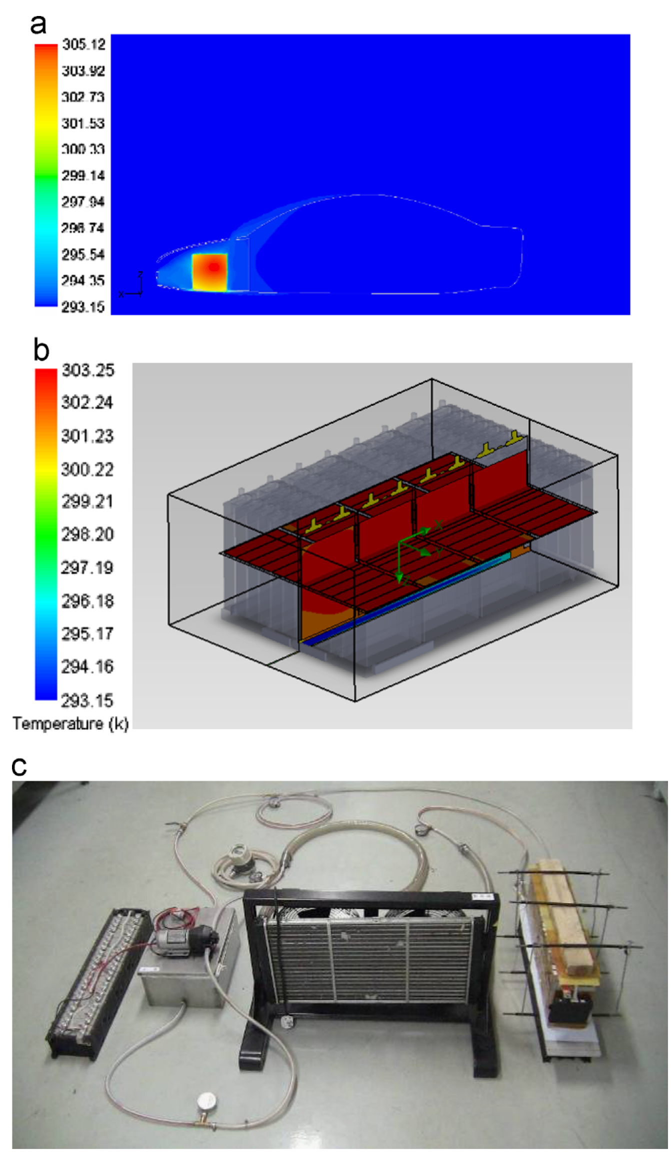


Fig. 1. Some studies on cooling system design of electric vehicle have been taken by the authors. (a) Temperature field distribution of electric vehicle basing on the nature air cooling. (b) Temperature field distribution of battery pack basing on the forced air cooling. (c) Liquid cooling system of battery module.

Nomenclature

Q	calorific value
c_p	specific heat capacity
m	quality
ΔT	temperature rising
P	thermal power
t	time
$\bar{v}$	velocity vector
p	pressure
ρ	density
μ	viscosity coefficient
E	total energy
u, v and w	the velocities of x, $y$and z direction
λ	thermal conductivity coefficient

little bit on key technology of electric vehicle for heat dissipation performance analysis.

This paper selects the battery pack as the study object (it has a total of 48 batteries, and includes 4 battery modules with 2 parallels and 6 series), and researches on the heat dissipation performance of battery pack with different structures and operation conditions, in order to offer a reference basis for heat flow field characteristic analysis and structure design.

It is organized as follows: Section 1 explains the thermal power determination test of 55 A h lithium-ion battery monomer on charge and discharge processing. Section 2 describes the thermal calculation method and heat dissipation performance indexes. Then, the content of heat flow field analysis with different structures will be explained in Section 3. Finally, Section 4 highlights the heat flow field analysis with different operation conditions and is followed by conclusions in Section 5.

2. Thermal power determination test of 55 A h lithium-ion battery monomer on charge and discharge processing

Lead-acid battery [61–63], nickel-zinc battery [63], and lithium-ion battery [63–64] are used as the power source of electric vehicle, now lithium-ion battery is as the main method of power source for electric vehicle [65–67].

Some researchers have studied the electrochemical properties [68–74] and thermal characteristics of lithium-ion battery: Pesaran [75] found that the best range of operating temperature for lithium-ion battery was between 25 °C and 40 °C; Bernardi [76] described the general energy balance for battery systems by assuming uniform temperature throughout the cell; Doyle [77] developed micro-scale model for the behavior of lithium/polymer/insertion cell under the isotropic condition; Chen [78], Newman [79], Pals [80], Doyle [81], Thomas [82] presented mathematical model focusing on the thermal management; Chen [83] examined the heat transfer within batteries using two-dimensional transient heat conduction analysis of the battery stack, with convective heat transfer at the battery boundaries; Srinivasan [84] studied electrochemical and thermal behavior of Li-ion cells employing two-dimensional unit layer.

This paper uses the heat insulation test to obtain the thermal power of battery monomer on charge and discharge processing for the heat source setting on simulation calculation.

Table 1
Thermal physical parameters of 55 A h lithium-ion battery monomer.

Battery component	Density (kg/m^3)	Thermal conductivity coefficient (W/m K)	Specific heat capacity (J/kg K)
Electric core	2123	30.6	913
Positive pole	2719	202.4	871
Negative pole	8978	387.6	381
Diaphragm	1008	0.3344	1978
Shell	8193	14.7	439.3

2.1. Thermal physical parameters of 55 A h lithium-ion battery monomer

Table1 shows the thermal physical parameters of 55 A h lithium-ion battery monomer: the density of electric core is 2123 kg/m^3, the thermal conductivity coefficient is 30.6 W/m K, and the specific heat capacity is 913 J/kg K.

2.2. Thermal power determination test of 55 A h lithium-ion battery monomer on charge and discharge processing

Fig. 2 shows the arrangement of temperature measuring point and the design of thermal insulation with 55 A h lithium-ion battery monomer, including 2 measuring points on bottom and 3 measuring points on side wall, heat insulation box has three layers of insulating material surround, in order to ensure good thermal insulation performance.

Fig. 3 shows the main test equipments, it uses CHALLENGE 600E to control the environment temperature of battery monomer, and the temperature range is 0–150 °C; it uses Digatron EVT 250–750-2*80 kW IGBT to charge and discharge for battery monomer, and the maximum current is 250 A; it uses Agilent 34970A to monitor the temperature of battery monomer, and the accuracy reaches 0.001 °C.

Calorific value could be expressed as

$$Q = c_p m \Delta T \tag{1}$$

where Q is the calorific value; $c_p$is the specific heat capacity; m is the quality; ΔT is the temperature rising.

So it can be derived that

$$P = \frac{c_p m \Delta T}{t} \tag{2}$$

where P is the thermal power; t is the time.

Constant temperature box is set to suitable temperature, the experimental processing is as follow: firstly, setting a certain charge rate up to 3.65 V; secondly, turning to constant-voltage charge, until 0.05 C cutoff; thirdly, setting this discharge rate down to 2.50 V.

When the environment temperature is 27 °C, and the charge and discharge rate is 1 C, Fig. 4 shows the temperature change curves of every measuring point at 100% SOC state, it could be seen that these temperature change curves approach each other, this means that the internal temperature of battery monomer is uniformity with thermal insulation environment. Therefore, for calculating the temperature rising of battery monomer, it just considers the average temperature rising of every measuring point.

When the environment temperature is 27 °C, and the charge and discharge rate is 1 C, Fig. 5 shows the average temperature curve of 55 A h lithium-ion battery monomer at 100% SOC state, combining with thermal physical parameters of 55 A h lithium-ion battery monomer, it could be obtained the thermal power on charge and discharge processing. As could be seen from Table 2, the average thermal power of 55 A h lithium-ion battery monomer is 6.51 W at 20 °C, 5.36 W at 27 °C, and 4.66 W at 40 °C, it is

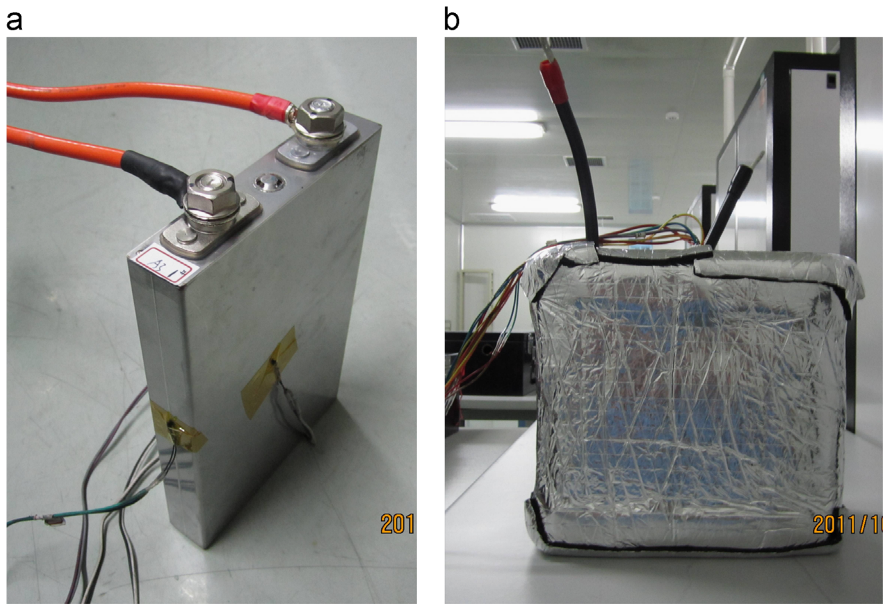


Fig. 2. The arrangement of temperature measuring point and the design of thermal insulation with 55 Ah lithium-ion battery monomer. (a) Temperature measuring point. (b) Heat insulation box.



Fig. 3. Main test equipments. (a) CHALLENGE 600E (b) Agilent 34970A. (c) Digatron EVT 250–750-2*80kW IGBT.

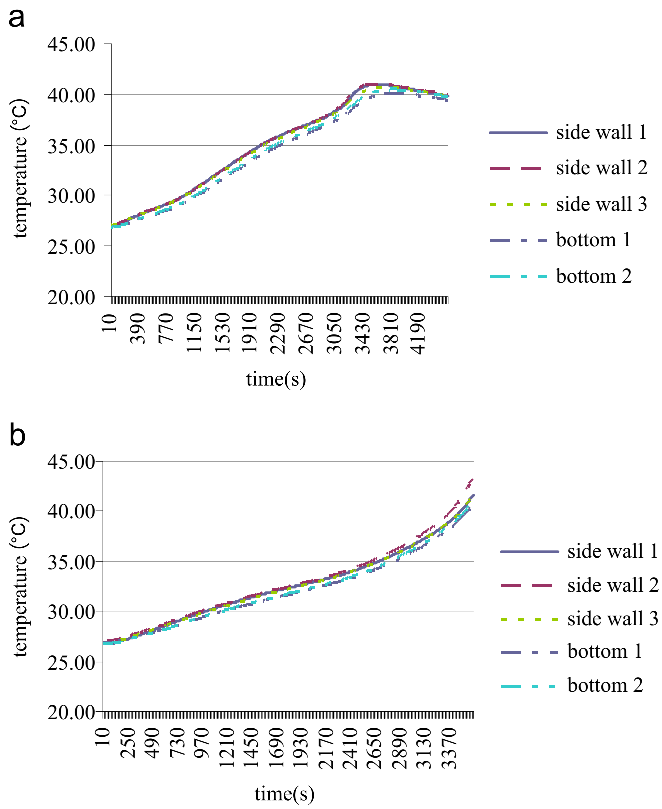


Fig. 4. When the environment temperature is 27 °C, and the charge and discharge rate is 1 C, the temperature change curves of every measuring point at 100% SOC state. (a) Charge processing. (b) Discharge processing.

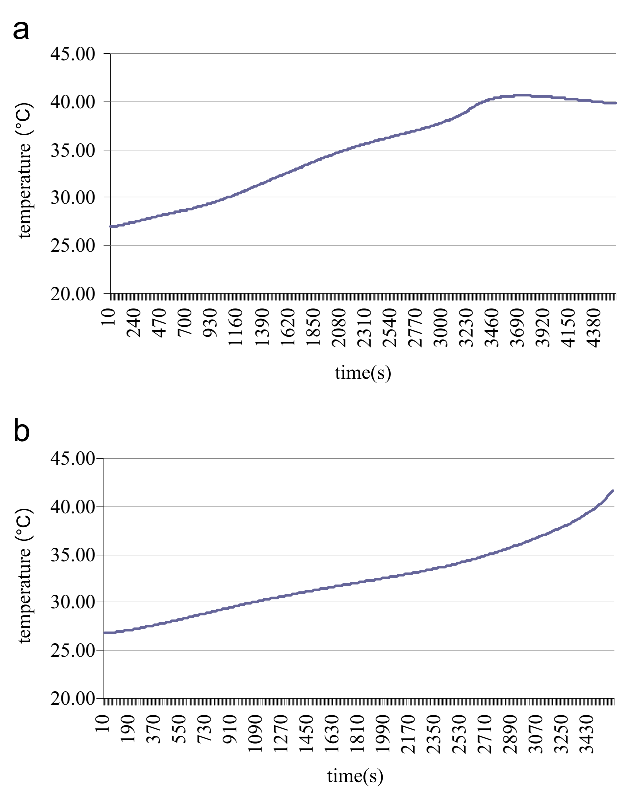


Fig. 5. When the environment temperature is 27 °C, the average temperature curve of 55 A h lithium-ion battery monomer on charge and discharge processing. (a) Charge processing. (b) Discharge processing.

Table 2
At different environment temperatures, the thermal power of 55 A h lithium-ion battery monomer on charge and discharge processing (W).

Temperature (°C)	Average thermal power on charge processing	Average thermal power on discharge processing	Average thermal power on charge and discharge processing
20	5.42	7.60	6.51
27	4.36	6.35	5.36
40	3.56	5.76	4.66

obvious that the average thermal power of 55 A h lithium-ion battery monomer decreasing along with environment temperature rising. As considering that the constant temperature box is not completely insulated, therefore, the measured average temperature rising of battery monomer is less than the temperature rising of actual thermal insulation; so the calculation value of thermal power is also slightly lower than the actual value.

3. Thermal calculation method and heat dissipation performance indexes

There are many methods to analyze the battery thermal behavior, in which experimental and numerical simulation are the most popular. Computational fluid dynamics (CFD) [85–86] and finite element methods (FEM) [87–88] are recommended for the investigation of the thermal systems.

Many thermal models are developed to describe temperature profiles and time evolution of temperature: Kim [89] formulated a three-dimensional thermal abuse model for lithium-ion battery; Catherino [90] performed a model to attempt studying the thermal runaway effect in lead-acid battery; Smith [91] used a complex one-dimensional thermal mathematical model with lumped parameters; Guo [92] also developed a three-dimensional thermal model for analyzing the temperature distribution of lithium-ion battery; Inui [93] simulated two-dimensional and three-dimensional temperature distributions in cylindrical and prismatic lithium-ion battery; Lee [94] used a three-dimensional model to investigate the effects of operating and ambient conditions on the thermal behavior furthered their study on a 42-V automotive electrical system; Chen [95] developed a detailed three-dimensional thermal model to examine the thermal behavior of lithium-ion battery; Wu [96] used a two-dimensional, transient heat-transfer model to simulate the temperature distribution.

This paper uses FloEFD as the CFD software to calculate the heat flow field data of battery pack basing on forced air cooling.

3.1. Mathematical model

Normally, the maximum velocity of airflow in battery pack is less than 400 km/h, it means less than 1/3 sound velocity, so the airflow in battery pack could be considered in incompressible flow, and the physical parameters of airflow are constant number. Combining with the phenomenon of air separation by complex structure of battery pack, it should be considered to the turbulent processing. The control equations are as follows:

Continuity equation

$$\nabla\bar{v}=0 \tag{3}$$

Momentum conservation equation

$$\frac{\partial\bar{v}}{\partial t}+(\bar{v}\nabla)\bar{v}=-\frac{\nabla p}{\rho}+\frac{\mu}{\rho}\nabla^2\bar{v} \tag{4}$$

Energy conservation equation

$$\rho c_p\left(\frac{\partial E}{\partial t}+u\frac{\partial E}{\partial x}+v\frac{\partial E}{\partial y}+w\frac{\partial E}{\partial z}\right)=\lambda\left(\frac{\partial^2 E}{\partial x^2}+\frac{\partial^2 E}{\partial y^2}+\frac{\partial^2 E}{\partial z^2}\right) \quad (5)$$

where $\overline{v}$ is the velocity vector, t is the time, p is the pressure, ρ is the density, μ is the viscosity coefficient, c_p is the specific heat, E is the total energy, u, v and w are the velocities of x, y and $z$direction, λ is the thermal conductivity coefficient.

3.2. Calculation method

Three-dimensional incompressible Navier-Stokes equations and standard $k-\varepsilon$ model are used, and SIMPLEC method is adapted to iterate.

3.3. Boundary condition

Free inlet boundary condition is considered, and the pressure is standard atmospheric pressure. The air-outlet is fan outlet boundary condition, and Fig. 6 shows the curve between fan pressure difference and flow rate: when the pressure difference between air-inlet and air-outlet is 125 Pa, the flow rate is 0.0028 m^3/s (10.8 m^3/h); when the pressure difference between air-inlet and air-outlet is 0 Pa, the flow rate is 0.0083 m^3/s (29.9 m^3/h), the battery pack includes two fans. It uses no-slip boundary condition as wall surface, and the speed is zero. The heat power of battery monomer depends on the specific example.

3.4. Heat dissipation performance indexes

Assessing the heat dissipation performance of battery pack cooling system has two main indexes: the maximum temperature rising and the maximum temperature difference (it defines the maximum difference value between battery pack temperature and environment temperature as maximum temperature rising, and the maximum value of battery pack internal temperature difference as maximum temperature difference). If the maximum temperature rising is too big, it means the environment temperature is relatively poor for battery pack regular work, and the heat generated by battery pack could not be effectively taken away through the cooling system; if the maximum temperature difference is too big, it means the temperature distribution uniformity of battery pack is poor, so the purpose of battery pack cooling system design is to reduce the maximum temperature rising and the maximum temperature difference.

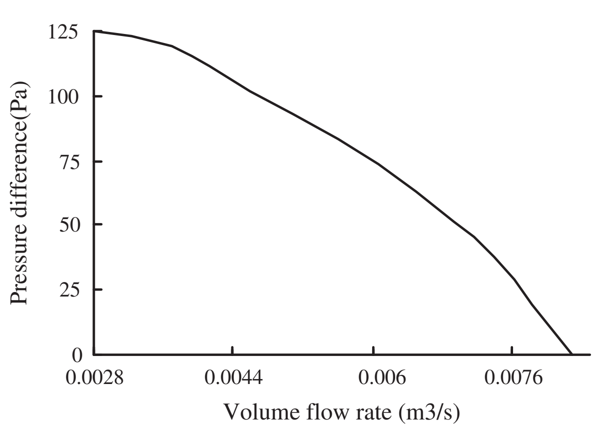


Fig. 6. The curve between fan pressure difference and flow rate.

4. Heat flow field analysis with different structures

Different structures and air-inlet and air-outlet modes will influence the heat dissipation performance of battery pack [97–102], many researchers have launched these studies.

Pesaran [103,104] presented that there are usually two ducts for the airflow to pass the battery pack, comparing with the serial airflow duct, the parallel airflow duct made the temperature uniformity of battery pack much better; Lin [105] pointed out two ways to ensure the airflow velocity uniform: regulating speed method and regulating pressure method, and given the optimal combination with each other; Mahamud [106] designed one thermal management system of periodic changing the flow direction of medium; J H Liang [107] put some obstacles in the air-inlet in order to control the flow rate of air into the different sub ducts; Zolot [108] used a parallel airflow scheme in a Toyota Prius hybrid electric vehicle, in order to cool the battery; Lou [109] designed a cinquefoil battery pack constituted by 5 long modules to enhance the heat transfer for batteries.

This paper studies the heat flow field characteristics of battery pack with different structures, including: longitudinal battery pack, horizontal battery pack, and changing the position of air-inlet and air-outlet.

4.1. Heat flow field analysis of longitudinal battery pack

4.1.1. Heat flow field analysis of longitudinal battery pack with no air cooling

When the environment temperature is 20 °C, Fig. 7 shows the temperature field distribution of longitudinal battery pack with no air cooling; the temperature of whole battery pack is relatively high and uniform. Table 3 shows that the maximum temperature rising and temperature difference of battery pack reduce along with environment temperature increasing, this is because the thermal power of battery pack decreasing along with environment temperature rising. Among them, the maximum temperature rising of battery pack at 40 °C is lower by 28.2% and 12.8% than 20 °C and 27 °C; the maximum temperature difference of battery pack at 40 °C is lower by 28.0% and 12.6% than 20 °C and 27 °C.

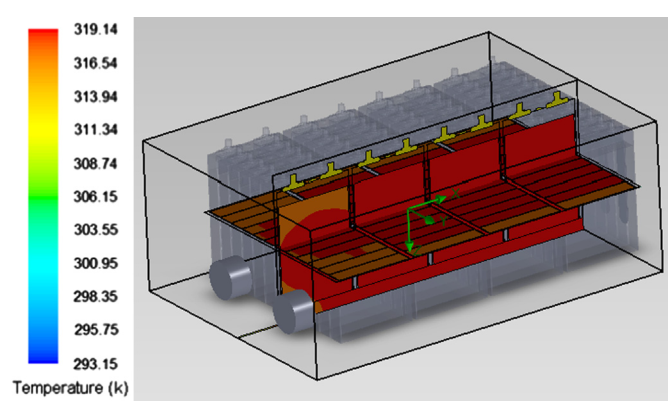


Fig. 7. When the environment temperature is 20 °C, the temperature field distribution of longitudinal battery pack with no air cooling.

Table 3
The heat flow field data of longitudinal battery pack with no air cooling at different environment temperatures.

Environment temperature (°C)	20	27	40
Maximum temperature rising (°C)	25.99	21.41	18.66

4.1.2. Heat flow field analysis of longitudinal battery pack basing on forced air cooling

The air-inlets are on the opposite position of fans, Fig. 8(a) shows that the high temperature area of longitudinal battery pack is in the central, and near the air-outlet, while the temperature of air-inlets is relatively low, so the temperature field distribution of longitudinal battery pack basing on forced air cooling is much difference to no air cooling. Airflow is inhaled from the air-inlet and heated by battery pack, and then the temperature of airflow rises, it eventually leads the airflow cooling capacity to decrease. Therefore, the purpose of reasonable airflow duct design should improve the airflow cooling capacity, especially near air-outlet, it is more important to improve airflow passing ability in order to decrease the temperature of airflow, as could be seen from Fig. 8 (b), the airflow mainly passes the top of battery pack but not through both sides, and near air-outlet, the speed of airflow is much higher. Table 4 shows the heat flow field data of longitudinal battery pack basing on forced air cooling at different environment temperatures, the flow rate and the average pressure drop between air-inlet and air-outlet both decrease along with environment temperature increasing. For the same airflow duct, the heat power of battery pack reduces along with environment temperature increasing, it eventually leads the maximum temperature rising and temperature difference of battery pack to reduce along with environment temperature increasing. Among them, the maximum temperature rising of battery pack at 40 °C is lower by 26.7% and 11.6% than 20 °C and 27 °C; the maximum temperature difference of battery pack at 40 °C is lower by 27.6% and 12.2% than 20 °C and 27 °C.

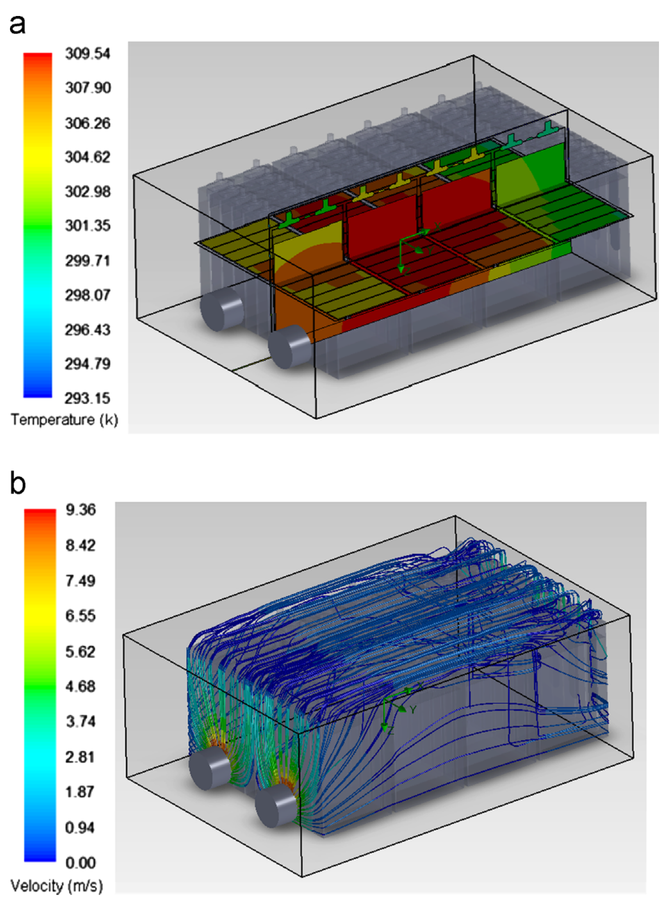


Fig. 8. The temperature field and velocity trace of longitudinal battery pack basing on forced air cooling at 20 °C. (a) Temperature field. (b) Velocity trace.

Table 4
The heat flow field data of longitudinal battery pack basing on forced air cooling at different environment temperatures.

Environment temperature (°C)	20	27	40
Flow rate (m^3/h)	34.15	33.50	32.21
Maximum temperature rising (°C)	16.39	13.58	12.01
Maximum temperature difference (°C)	12.00	9.90	8.69

4.2. The comparison of heat flow field between longitudinal battery pack and horizontal battery pack

4.2.1. Heat flow field analysis of Horizontal battery pack basing on forced air cooling

It could improve the heat dissipation capability by shorting the airflow path in order to improve airflow passing ability. For example, it could change the above longitudinal battery pack into a horizontal battery pack, and the air-inlets are also on the opposite position of fans. Fig. 9 shows that the high temperature area of horizontal battery pack is in the central, and near the air-outlet; the low temperature area is on the top of battery pack, and near the air-inlet. Combining with velocity trace distribution, it could be seen that the airflow along with the top and two sides of horizontal battery pack is uniform, then avoiding the problem of little airflow passing through two sides of battery pack. As could be seen from Table 5, the flow rate and the average pressure drop between air-inlet and air-outlet both decrease along with environment temperature increasing, and the maximum temperature

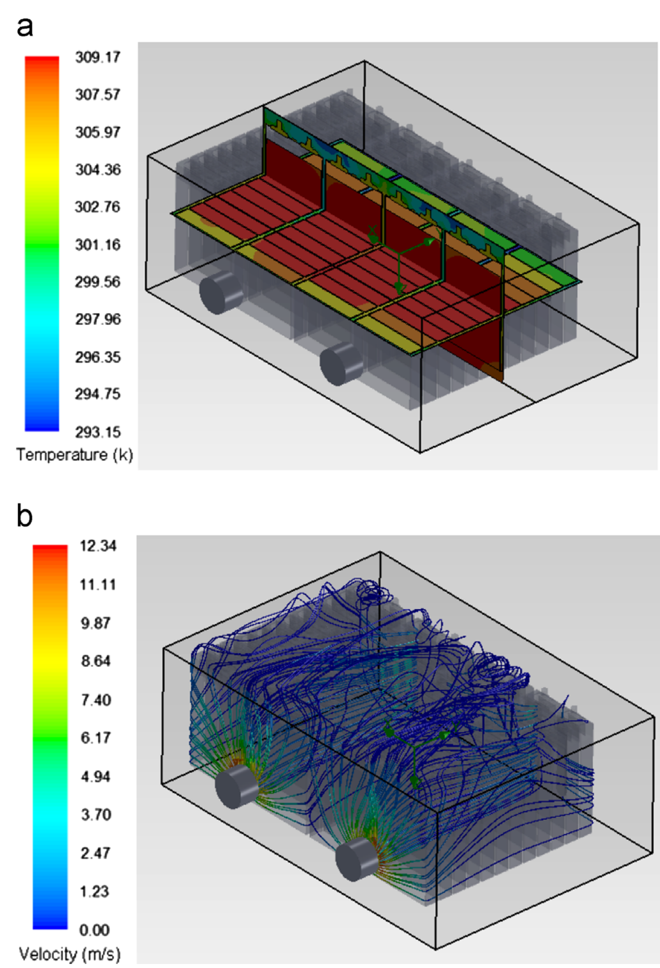


Fig. 9. The temperature field and velocity trace of horizontal battery pack basing on forced air cooling at 20 °C. (a) Temperature field. (b) Velocity trace.

Table 5
The heat flow field data of horizontal battery pack basing on forced air cooling at different environment temperatures.

Environment temperature (°C)	20	27	40
Flow rate (m^3/h)	34.77	34.12	32.80
Maximum temperature rising (°C)	16.02	13.31	11.83
Maximum temperature difference (°C)	11.05	9.18	8.19
Average pressure drop (Pa)	89	87	84

Table 6
The comparison of heat flow field characteristics between longitudinal battery pack and horizontal battery pack.

	Longitudinal battery pack	Horizontal battery pack
Flow rate (m^3/h)	34.15	34.77
Maximum temperature rising (°C)	16.39	16.02
Maximum temperature difference (°C)	12.00	11.05
Average pressure drop (Pa)	76	89

rising and temperature difference of battery pack reduce along with environment temperature increasing too. Among them, the maximum temperature rising of horizontal battery pack at 40 °C is lower by 26.2% and 11.1% than 20 °C and 27 °C; the maximum temperature difference of horizontal battery pack at 40 °C is lower by 25.9% and 10.8% than 20 °C and 27 °C.

4.2.2. *The comparison of heat flow field characteristics between longitudinal battery pack and horizontal battery pack*

When the environment temperature is 20 °C, Table 6 shows the comparison of heat flow field characteristics between longitudinal battery pack and horizontal battery pack, comparing with longitudinal battery pack, the flow rate and the average pressure drop between air-inlet and air-outlet of horizontal battery pack both increase, while the maximum temperature rising and temperature difference of horizontal battery pack both decrease. Among them, the maximum temperature rising of horizontal battery pack is lower by 22.6% than longitudinal battery pack; the maximum temperature difference of horizontal battery pack is lower by 7.9% than longitudinal battery pack.

4.3. *Heat flow field analysis of horizontal battery pack with different air-inlet and air-outlet modes*

4.3.1. *Adding air-inlets on both sides of battery pack*

Different air-inlet and air-outlet modes of horizontal battery pack basing on forced air cooling have different heat dissipation performance, when the environment temperature is 20 °C, Fig. 10 shows that the high temperature region of battery pack with air-inlets on both sides decreases, and the maximum temperature of battery pack also reduces; the airflow distribution is more uniform after adding air-inlets on both sides of battery pack, and it will improve the heat dissipation performance of airflow, among them, the maximum temperature rising and the maximum temperature difference of horizontal battery pack with air-inlets on both sides are lower by 0.8% and 11.8% than the original mode. As could be seen from Table 7, while the battery pack adding air-inlets on both sides, the flow rate and the average pressure drop between air-inlet and air-outlet both decrease along with environment temperature increasing, and the maximum temperature rising and temperature difference of battery pack reduce along with environment temperature increasing too, among them, the maximum temperature rising of battery pack at 40 °C is lower by 26.9% and 11.9% than 20 °C and 27 °C; the maximum temperature difference of battery pack at 40 °C is lower by 26.8% and 11.9% than 20 °C and 27 °C.

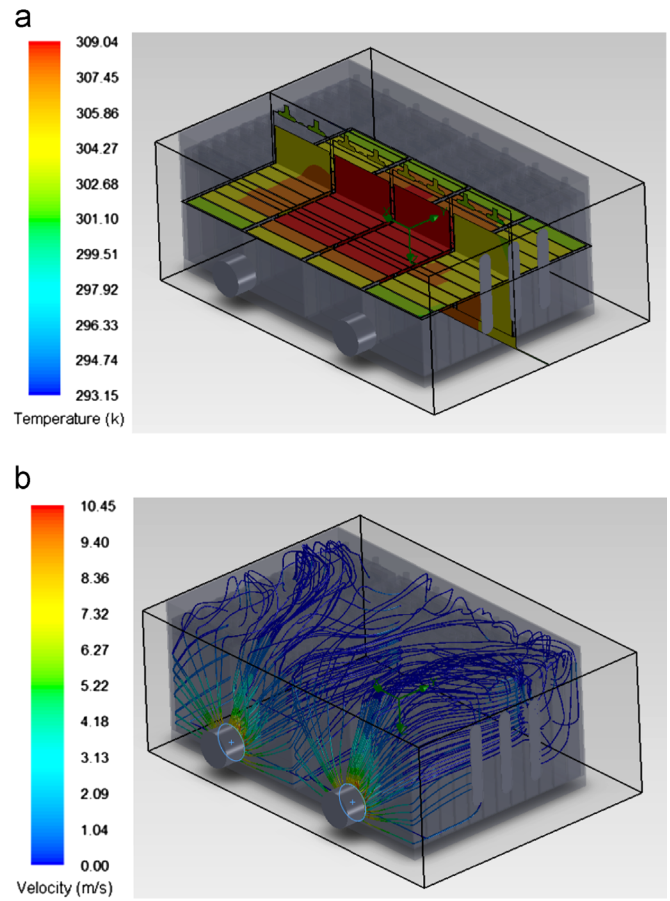


Fig. 10. Adding air-inlets on both sides of battery pack, the temperature field and velocity trace of horizontal battery pack at 20 °C. (a) Temperature field. (b) Velocity trace.

Table 7
Adding air-inlets on both sides of battery pack, the heat flow field data of horizontal battery pack at different environment temperatures.

Environment temperature (°C)	20	27	40
Flow rate (m^3/h)	34.65	34.00	32.68
Maximum temperature rising (°C)	15.89	13.18	11.61
Maximum temperature difference (°C)	9.75	8.09	7.13
Average pressure drop (Pa)	78	76	73

4.3.2. *Moving fans upwards*

When the environment temperature is 20 °C, Fig. 11 shows the temperature field and velocity trace of horizontal battery pack with moving fans upwards, it could be seen that the airflow passes through the top and both sides of battery pack; the flow rate below fans is very low, so it would reduce the airflow cooling capacity. Table 8 shows that the flow rate and the average pressure drop between air-inlet and air-outlet both decrease along with environment temperature increasing, and the maximum temperature rising and temperature difference of battery pack also reduce.

4.3.3. *Adding horizontal air-inlets on the top of battery pack*

When the environment temperature is 20 °C, Fig. 12 shows the temperature field and velocity trace of horizontal battery pack with horizontal air-inlets on the top of battery pack, it could be seen that the airflow mainly passes the top of battery pack but not through both sides, the airflow inhaled from horizontal air-inlets on the top of battery pack passes through fans quickly, which reduces the temperature near the fans. Table 9 shows that the flow

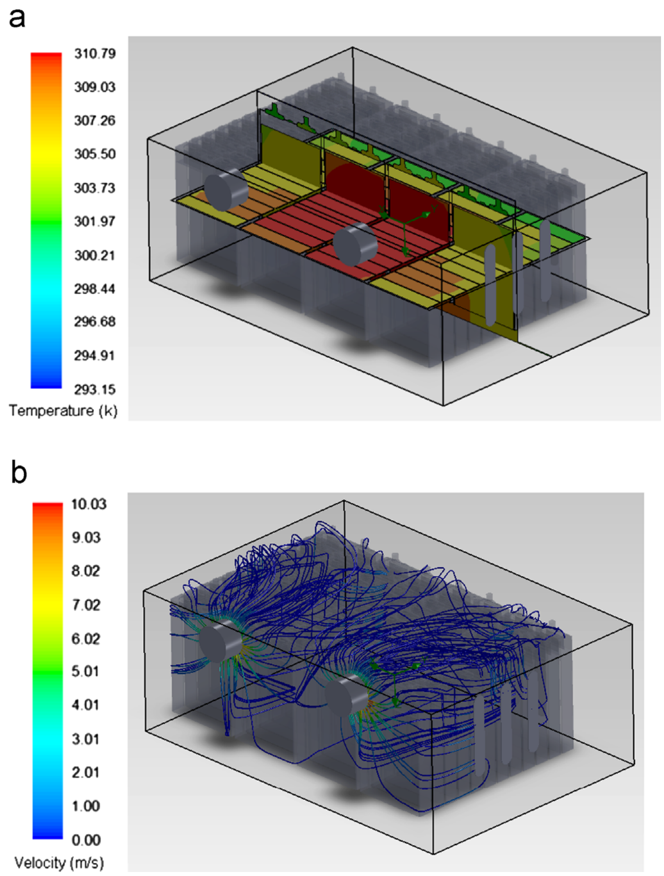


Fig. 11. Moving fans upwards, the temperature field and velocity trace of horizontal battery pack at 20 °C. (a) Temperature field. (b) Velocity trace.

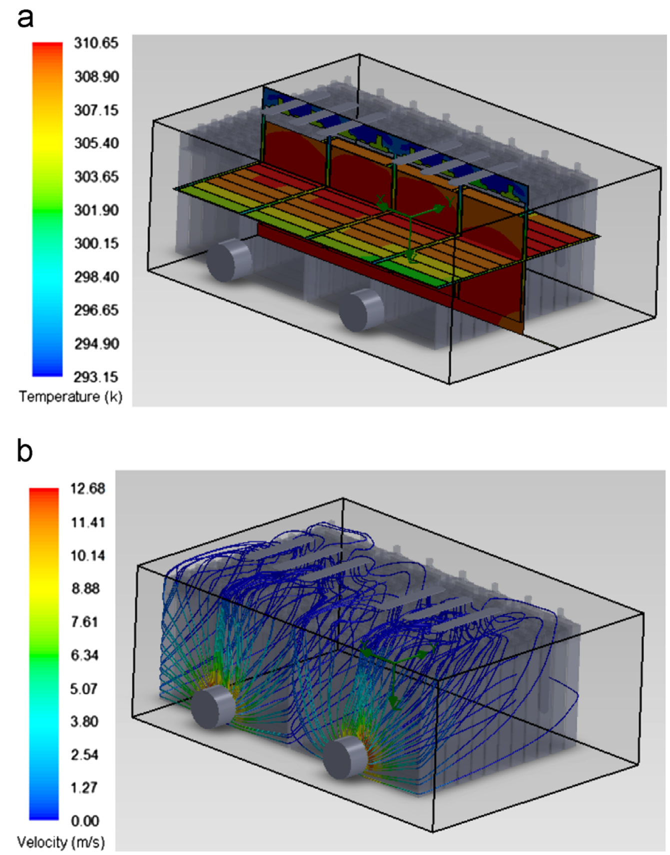


Fig. 12. Adding horizontal air-inlets on the top of battery pack, the temperature field and velocity trace of horizontal battery pack at 20 °C. (a) Temperature field. (b) Velocity trace.

Table 8
Moving fans upwards, the heat flow field data of horizontal battery pack at different environment temperatures.

Environment temperature (°C)	20	27	40
Flow rate (m^3/h)	34.48	34.06	32.54
Maximum temperature rising (°C)	17.64	14.60	12.89
Maximum temperature difference (°C)	11.80	9.79	8.61
Average pressure drop (Pa)	70	69	67

Table 9
Adding horizontal air-inlets on the top of battery pack, the heat flow field data of horizontal battery pack at different environment temperatures.

Environment temperature (°C)	20	27	40
Flow rate (m^3/h)	34.85	34.18	32.86
Maximum temperature rising (°C)	17.50	14.46	12.70
Maximum temperature difference (°C)	13.23	10.91	9.55
Average pressure drop (Pa)	85	84	81

rate and the average pressure drop between air-inlet and air-outlet both decrease along with environment temperature increasing, and the maximum temperature rising and temperature difference of battery pack also reduce.

4.3.4. Adding longitudinal air-inlets on the top of battery pack

Changing the horizontal air-inlet into longitudinal air-inlet, Fig. 13 shows the temperature field and velocity trace of horizontal battery pack with longitudinal air-inlets on the top of battery pack, and they are similar to horizontal air-inlet. Table 10 shows that the flow rate and the average pressure drop between air-inlet and air-outlet both decrease along with environment temperature increasing, and the maximum temperature rising and temperature difference of battery pack also reduce.

4.3.5. The comparison of heat flow field characteristics among different air-inlet and air-outlet modes of horizontal battery pack basing on forced air cooling

When the environment temperature is 20 °C, Table 11 shows the comparison of heat flow field characteristics among different air-inlet and air-outlet modes of horizontal battery pack basing on forced air cooling, the maximum temperature rising and temperature difference of battery pack with air-inlets on both sides are maximum, and the mode with moving fans upwards is minimum. Among them, the maximum temperature rising of battery pack with air-inlets on both sides is lower by 9.9%, 9.2% and 8.9% than the mode with moving fans upwards, the mode with horizontal air-inlets on the top and the mode with longitudinal air-inlets on the top; the maximum temperature difference of battery pack with air-inlets on both sides is lower by 17.4%, 26.3% and 25.6% than the mode with moving fans upwards, the mode with horizontal air-inlets on the top and the mode with longitudinal air-inlets on the top. The flow rate and the average pressure drop between air-inlet and air-outlet of horizontal air-inlets and longitudinal air-inlets are same, and their flow rate is higher by 0.2 m^3/h and 0.37 m^3/h than the mode with air-inlets on both sides and the mode with moving fans upwards, their average pressure drop between air-inlet and air-outlet is higher by 7 Pa and 15 Pa than the mode with air-inlets on both sides and the mode with moving fans upwards, so the maximum temperature rising and temperature difference of battery pack are not only relevant to the flow

rate, but also related to the airflow duct structure, selecting battery pack with air-inlets on both sides is more conducive to the forced air cooling.

5. Heat flow field analysis with different operation conditions

Different operation conditions will influence the heat flow field characteristics of battery pack [110–117] too, batteries may work in some cases as follows: high temperature [118–121], low temperature [118–121], over-charge [122], over-discharge [122], high rate charge and discharge [122]. So it is necessary to carry out the study of heat flow field characteristics of battery pack with different operation conditions.

Pesaran [123] analyzed the effects of ambient temperature ranges on the battery packs; Hallaj [124] analyzed the effects of high temperature on a lithium-ion battery through both theoretical (thermal modeling) and experimental analysis; Cosley [125] compared different methods of keeping the VLRA (valve-regulated lead-acid battery) temperatures within desired ranges through air conditioning; Ramadass [126] did a capacity fade analysis for lithium-ion battery and elucidated that 31% SOC and 36% SOC of the initial capacity were lost after 800 charge and discharge cycles which were operated at 25 °C and 45 °C; Li [127] also pointed out that the cycle life of lithium-ion battery is 3323 cycles at 45 °C, but 1037 cycles at 60 °C; Hong [128] indicated that the entropy change could contribute more than 50% of the total heat generated at the 1 C discharge rate; Sato [129] reported the thermal behavior of lithium-ion batteries for EV through thermodynamic analyses, and examined the heat absorption and generation processes at different charging and discharging rates.

This part selects the battery pack with air-inlets on both sides as the research object, and studies the heat flow field characteristics of battery pack with different operation conditions, including: SOC state, charge and discharge rate, and practical operation condition.

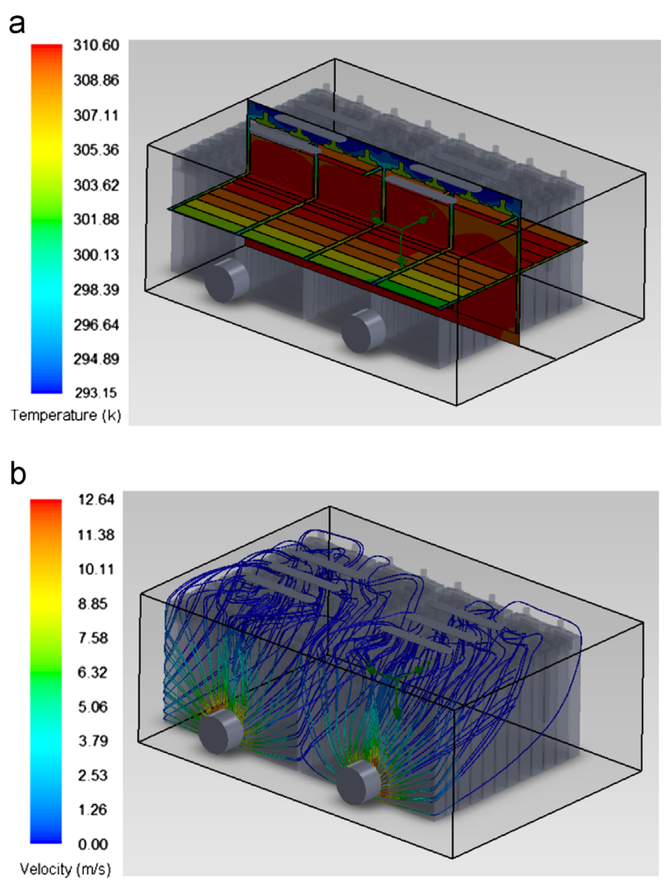


Fig. 13. Adding longitudinal air-inlets on the top of battery pack, the temperature field and velocity trace of horizontal battery pack at 20 °C. (a) Temperature field. (b) Velocity trace.

Table 10
Adding longitudinal air-inlets on the top of battery pack, the heat flow field data of horizontal battery pack at different environment temperatures.

Environment temperature (°C)	20	27	40
Flow rate (m^3/h)	34.85	34.18	32.86
Maximum temperature rising (°C)	17.45	14.43	12.62
Maximum temperature difference (°C)	13.31	10.99	9.59

5.1. *Heat flow field analysis at different SOC states*

5.1.1. *The thermal power of 55 A h lithium-ion battery at different SOC states*

When the environment temperature is 20 °C, and the charge and discharge rate is 1 C, Fig. 14 shows the average temperature curve of 55 A h lithium-ion battery monomer at 70% SOC state, Table 12 shows the thermal power of 55 A h lithium-ion battery monomer at different SOC states. The average thermal power of 55 A h lithium-ion battery monomer is 6.25 W at 70% SOC state, 6.87 W at 80% SOC state, 7.19 W at 90% SOC state, and 6.51 W at 100% SOC state, it is obvious that the average thermal power of 55 A h lithium-ion battery monomer increasing along with SOC state rising.

5.1.2. *Heat flow field analysis at 70% SOC state*

Fig. 15 shows the temperature field and velocity trace of battery pack with air-inlets on both sides at 70% SOC state, comparing with 100% SOC state, the temperature field distribution and velocity trace are basically the same except the numerical value. As could be seen from Table 13, the maximum temperature rising and temperature difference of battery pack are 15.28 °C and 9.38 °C.

5.1.3. *The comparison of heat flow field characteristics at different SOC states*

Table 14 shows the heat flow field characteristics comparison of battery pack with air-inlets on both sides at different SOC states, as could be seen that the flow rate of battery pack at 70% SOC state is maximum; the maximum temperature rising and temperature difference of battery pack at 70% SOC state is minimum, and 90%

Table 11
The comparison of heat flow field characteristics among different air-inlet and air-outlet modes of horizontal battery pack basing on forced air cooling.

	Air-inlets on both sides	Moving fans upwards	Horizontal air-inlets on the top	Longitudinal air-inlets on the top
Flow rate (m^3/h)	34.65	34.48	34.85	34.85
Maximum temperature rising (°C)	15.89	17.64	17.50	17.45
Maximum temperature difference (°C)	9.75	11.80	13.23	13.11

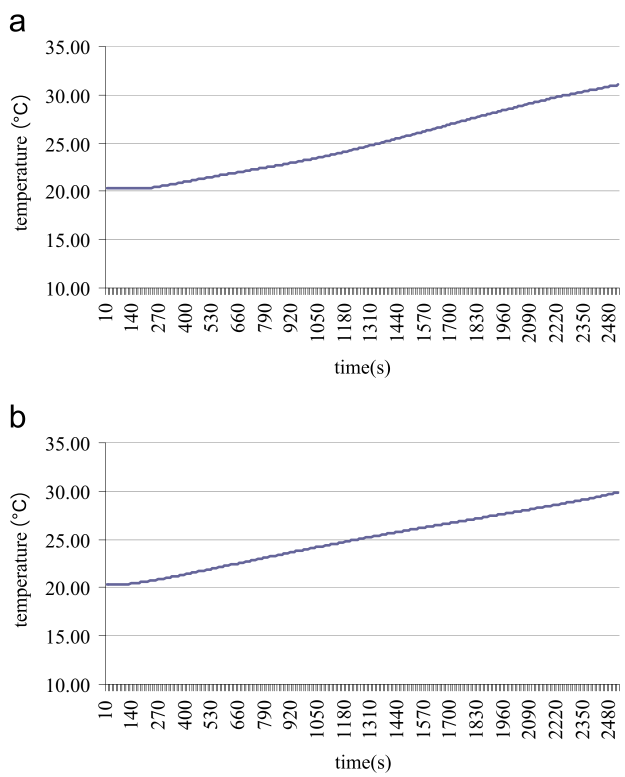


Fig. 14. The average temperature curve of 55 A h lithium-ion battery monomer at 70% SOC state. (a) Charge processing. (b) Discharge processing.

Table 12
On charge and discharge processing, the thermal power of 55 A h lithium-ion battery monomer at different SOC states (W).

SOC state (%)	Average thermal power on charge processing	Average thermal power on discharge processing	Average thermal power on charge and discharge processing
70	6.60	5.90	6.25
80	6.86	6.88	6.87
90	7.11	7.27	7.19
100	5.42	7.60	6.51

SOC state is maximum; the maximum temperature rising and temperature difference of battery pack at 100% SOC state is between 70% and 80% SOC state.

5.2. Heat flow field analysis at different charge and discharge rates

5.2.1. The thermal power of 55 A h lithium-ion battery monomer at different charge and discharge rates

When the environment temperature is 20 °C, and the SOC state is 100%, Fig. 16 shows the average temperature curve of 55 A h lithium-ion battery monomer at 0.5 C charge and discharge rate, Table 15 shows the thermal power of 55 A h lithium-ion battery monomer at different charge and discharge rates. The average thermal power of 55 A h lithium-ion battery monomer is 2.31 W at 0.5 C, 3.42 W at 0.6 C, 5.00 W at 0.8 C, 6.51 W at 1 C, 8.44 W at 1.2 C, 12.83 W at 1.5 C, and 19.17 W at 2 C, it is obvious that the average thermal power of 55 A h lithium-ion battery monomer increasing along with charge and discharge rate rising.

5.2.2. Heat flow field analysis at 0.5 C charge and discharge rate

Fig. 17 shows the temperature field and velocity trace of battery pack with air-inlets on both sides at 0.5 C charge and discharge rate, comparing with 1 C charge and discharge rate, the temperature field distribution and velocity trace are basically the same except the numerical value. As could be seen from Table 16, the maximum temperature rising and temperature difference of battery pack are 5.64 °C and 3.45 °C.

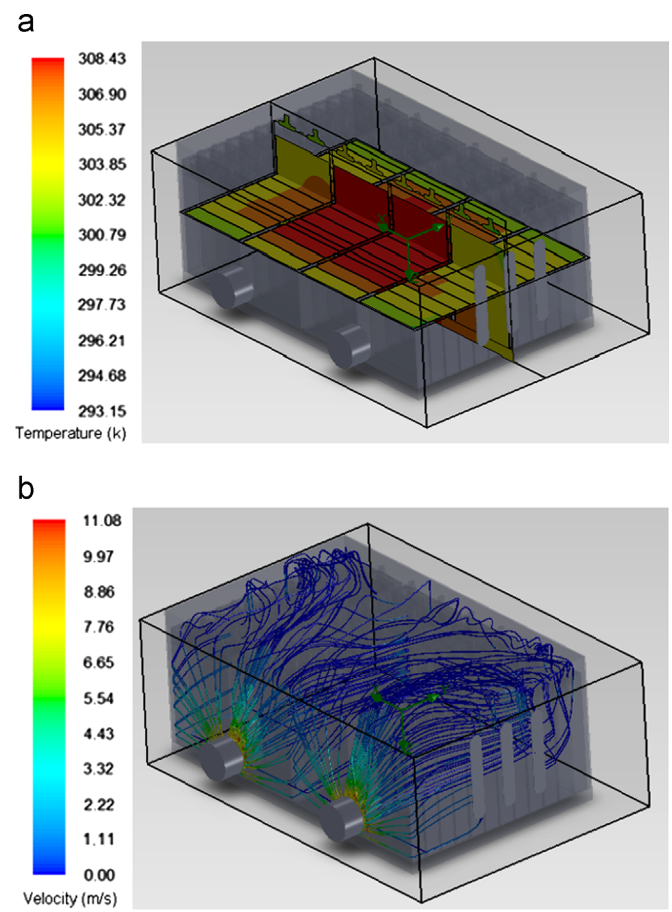


Fig. 15. The temperature field and velocity trace of battery pack with air-inlets on both sides at 70% SOC state (a) Temperature field. (b) Velocity trace.

Table 13
The data of heat flow field with air-inlets on both sides at 70% SOC state.

Parameter	Date
Flow rate (m^3/h)	34.68
Maximum temperature rising (°C)	15.28
Maximum temperature difference (°C)	9.38
Average pressure drop (Pa)	78

Table 14
The heat flow field characteristics comparison of battery pack with air-inlets on both sides at different SOC states.

SOC state (%)	Flow rate (m^3/h)	Maximum temperature rising (°C)	Maximum temperature difference (°C)	Average pressure drop (Pa)
70	34.68	15.28	9.38	78
80	34.59	16.82	10.32	78
90	34.56	17.59	10.79	77
100	34.65	15.89	9.75	78

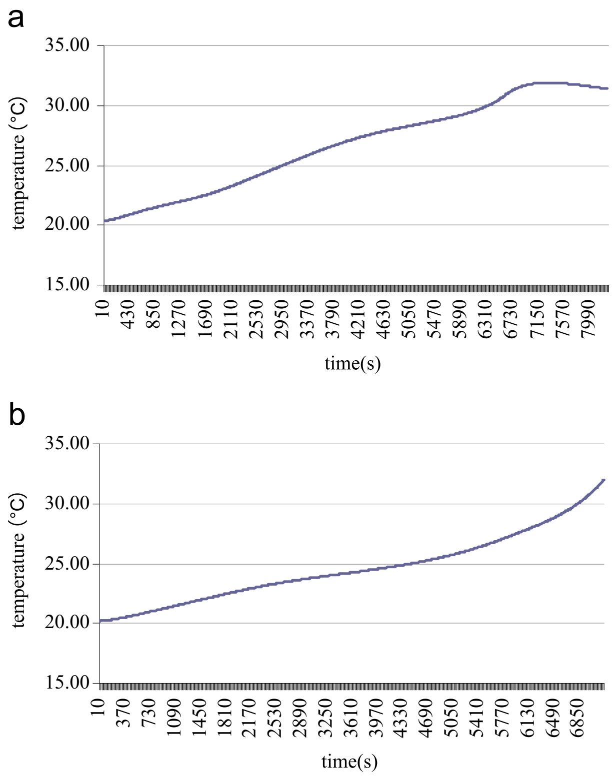


Fig. 16. The average temperature curve of 55 A h lithium-ion battery monomer at 0.5 C charge and discharge rate. (a) Charge processing. (b) Discharge processing.

Table 15
The thermal power of 55 A h lithium-ion battery monomer at different charge and discharge rates (W).

Charge and discharge rate (C)	Average thermal power on charge processing	Average thermal power on discharge processing	Average thermal power on charge and discharge processing
0.5	2.06	2.55	2.31
0.6	2.95	3.89	3.42
0.8	4.31	5.69	5.00
1	5.42	7.60	6.51
1.2	6.62	10.25	8.44
1.5	10.06	15.60	12.83
2	14.44	23.89	19.17

5.2.3. The comparison of heat flow field characteristics at different charge and discharge rates

Table 17 shows the heat flow field characteristics comparison of battery pack with air-inlets on both sides at different charge and discharge rates, as could be seen that the flow rate and the average pressure drop between air-inlet & air-outlet both decrease along with charge and discharge rate increasing, while the maximum temperature rising and temperature difference of battery pack increase. Among them, the maximum temperature rising of battery pack at 0.5 C charge and discharge rate is lower by 32.3%, 53.8%, 64.5%, 72.7%, 82.2% and 88.2% than 0.6 C, 0.8 C, 1 C, 1.2 C, 1.5 C and 2 C; the maximum temperature difference of battery pack at 0.5 charge and discharge rate is lower by 32.5%, 53.9%, 64.6%, 72.8%, 82.2% and 88.2% than 0.6 C, 0.8 C, 1 C, 1.2 C, 1.5 C and 2 C.

5.3. Heat dissipation performance analysis with practical operation condition

This part selects the battery pack with air-inlets on both sides as the research object, Fig. 18 shows the curve of electric current following the battery pack work (battery pack work time is 3000 s), as considering the practical operation condition of battery pack is very complicated, it is separately statistics for charge and discharge processing. As could be seen from Table 18, basing on

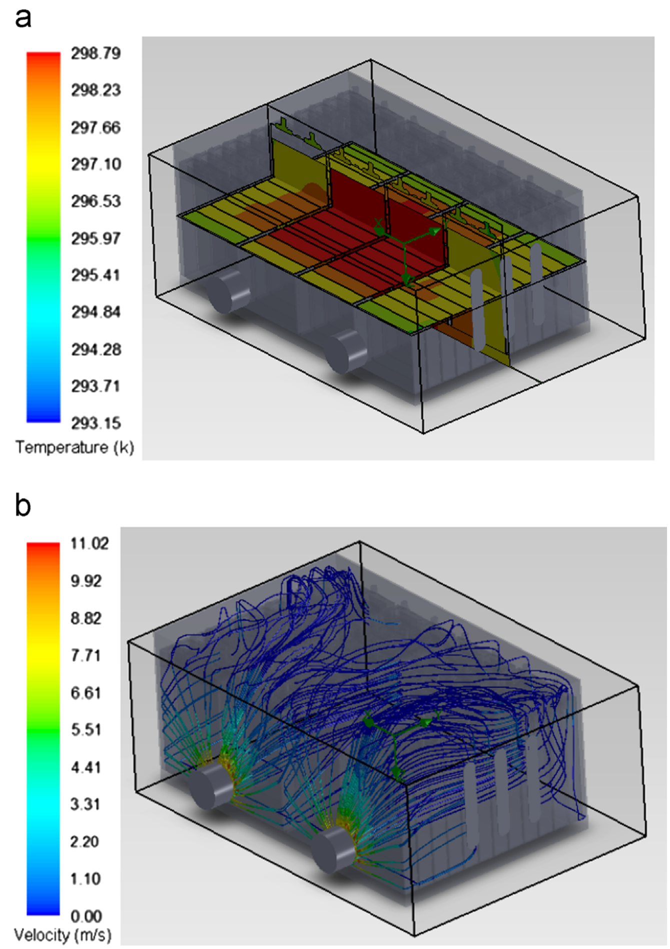


Fig. 17. The temperature field and velocity trace of battery pack with air-inlets on both sides at 0.5 C charge and discharge rate. (a) Temperature field. (b) Velocity trace.

Table 16
The data of heat flow field with air-inlets on both sides at 0.5 C charge and discharge rate.

Parameter	Date
Flow rate (m^3/h)	35.24
Maximum temperature rising (°C)	5.64
Maximum temperature difference (°C)	3.45
Average pressure drop (Pa)	79

Table 17
The heat flow field characteristics comparison of battery pack with air-inlets on both sides at different charge and discharge rates.

Charge and discharge rate (C)	Flow rate (m^3/h)	Maximum temperature rising (°C)	Maximum temperature difference (°C)	Average pressure drop (Pa)
0.5	35.24	5.64	3.45	79
0.6	35.06	8.33	5.11	79
0.8	34.85	12.20	7.48	78
1	34.65	15.89	9.75	78
1.2	34.38	20.69	12.70	77
1.5	33.80	31.72	19.42	75

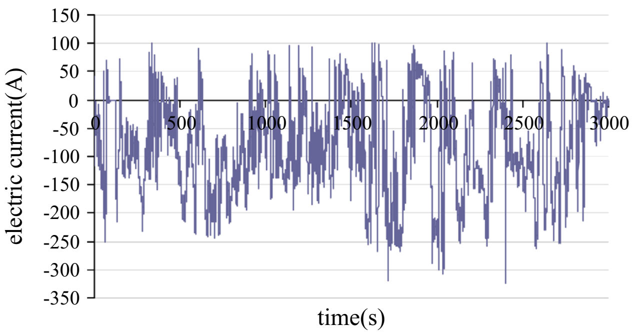


Fig. 18. The curve of electric current following the battery pack work.

Table 18
Practical operation condition of battery pack.

	Charge processing	Discharge processing
Average electric current (A)	56.05	87.88
Time (S)	513	2487
Charge and discharge rate (C)	0.51	0.80
Average heat power (W)	2.06	5.69

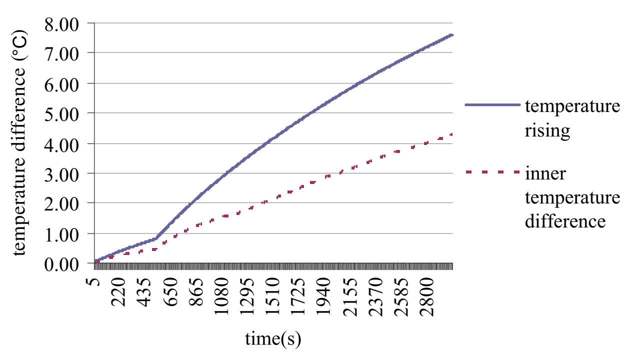


Fig. 19. The curves of temperature rising and inner temperature difference following the battery pack practical work.

the practical operation of battery pack, the average charge rate is 0.51 C, and the average heat power of battery monomer is 2.06 W; the average discharge rate is 0.80 C, and the average heat power of battery monomer is 5.69 W.

Fig. 19 shows the curves of temperature rising and inner temperature difference following the battery pack practical work, it could be seen that the maximum temperature rising of battery pack is 7.61 °C, and the maximum temperature difference of battery pack is 4.29 °C. Comparing with steady state condition, the charge and discharge rate is between 0.5 C and 0.8 C, and the maximum temperature rising and maximum temperature difference of battery pack rise sharply changing from charge processing into discharge processing, at the end time of discharge processing, those values reach the maximum.

6. Conclusions

Through the above research, the conclusions are as follows:

(1) The thermal power of battery monomer on charge and discharge processing is the reference for the heat source setting on the simulation calculation of battery pack, this study shows that: the average thermal power of 55 A h lithium-ion battery decreases along with environment temperature rising, SOC state decreasing and charge and discharge rate falling;
(2) changing the longitudinal battery pack into the horizontal battery pack, it could improve the heat dissipation capability by shorting the airflow path;
(3) comparing of heat flow field characteristics among different air-inlet and air-outlet modes of horizontal battery pack basing on forced air cooling, the result shows that: the maximum temperature rising and temperature difference of battery pack are not only relevant to the flow rate, but also related to the airflow duct structure, selecting battery pack with air-inlets on both sides is more conducive to the forced air cooling;
(4) comparison of heat flow field characteristics at different SOC states, the flow rate of battery pack at 70% SOC state is maximum; the maximum temperature rising and temperature difference of battery pack at 70% SOC state are minimum, and that of 90% SOC state are maximum; the maximum temperature rising and temperature difference of battery pack at 100% SOC state are between 70% and 80% SOC state;
(5) comparison of heat flow field characteristics at different charge and discharge rates, the flow rate and the average pressure drop between air-inlet and air-outlet both decrease along with charge and discharge rate increasing, while the maximum temperature rising and temperature difference of battery pack increase;
(6) considering the practical operation condition of battery pack is very complicated, it is separately statistics for the average heat power of battery monomer, on charge and discharge processing, the average heat power of battery monomer are 2.06 W and 5.69 W, and the maximum temperature rising and maximum temperature difference of battery pack are 7.61 °C and 4.29 °C.

Acknowledgments

This work was supported by the National “863” High-Tech Research and the Development Plan of China (2011AA11A220); the Science and Technology Achievement Transformation project of Jiangsu Provincial (BA2010050).

References

[1] Siang FT, Chee WT. A review of energy sources and energy management system in electric vehicles. Renewable and Sustainable Energy Reviews 2013;20:82–102.
[2] Huang KD, Tang SC, Chang WC. Energy-saving hybrid vehicle using a pneumatic-power system. Applied Energy 2005;81(1):1–18.
[3] Fayaz H, Saidur R, Razali N. An overview of hydrogen as a vehicle fuel. Renewable and Sustainable Energy Reviews 2012;16(8):5511–28.
[4] Skerlos SJ, Winebrake JJ. Targeting plug-in hybrid electric vehicle policies to increase social benefits. Energy Policy 2010;38(2):705–8.
[5] Amjad S, Neelakrishnan S, Rudramoorthy R. Review of design considerations and technological challenges for successful development and deployment of plug-in hybrid electric vehicles. Renewable and Sustainable Energy Reviews 2010;14(3):1104–10.
[6] Nahman J, Tanaskovic M. Calculation of the ampacity of medium voltage self-supporting cable bunch. Electric Power Systems Research 2012;93:106–12.
[7] Wada M. Research and development of electric vehicles for clean transportation. Journal of Environmental Sciences China 2009;21(6):745–9.
[8] Peng MH, Liu L, Jiang. CW. A review on the economic dispatch and risk management of the large-scale plug-in electric vehicles (PHEV)-penetrated power systems. Renewable and Sustainable Energy Reviews 2012;16:1508–15.
[9] Bradley TH, Frank AA. Design demonstrations and sustainability impact assessments for plug-in hybrid electric vehicles. Renewable and Sustainable Energy Reviews 2009;13(1):115–28.
[10] Silva C, Baptista P, Tomas M. Plug-in hybrid fuel cell vehicles market penetration scenarios. International Journal of Hydrogen Energy 2010;35(18):10024–30.

[11] Avadikyan A, Llerena P. A real options reasoning approach to hybrid vehicle investments. Technological Forecasting and Social Change 2010;77:649–61.
[12] Choi H, Oh I. Analysis of product efficiency of hybrid vehicles and promotion policies. Energy Policy 2010;38(5):2262–71.
[13] Richardson DB. Electric vehicles and the electric grid: a review of modeling approaches, Impacts, and renewable energy integration. Renewable and Sustainable Energy Reviews 2013;19:247–54.
[14] Weinert J, Ogden J, Sperling D. The future of electric two-wheelers and electric vehicles in China. Energy Policy 2008;36(7):2544–55.
[15] Poursamad A, Montazeri M. Design of genetic-fuzzy control strategy for parallel hybrid electric vehicles. Control Engineering Practice 2008;16(7):861–73.
[16] Schell A, Peng H, Tran D. Modeling and control strategy development for fuel cell electric vehicles. Annual Reviews in Control 2005;29(1):159–68.
[17] Bradley TH, Quinn CW. Analysis of plug-in hybrid electric vehicle utility factors. Journal of Power Sources 2010;195(16):5399–408.
[18] Moura PS, Almeida AT. Multi-objective optimization of a mixed renewable system with demand-side management. Renewable and Sustainable Energy Reviews 2010;14(5):1461–8.
[19] Williford RE, Viswanathan VV, Zhang JG. Effects of entropy changes in anodes and cathodes on the thermal behavior of lithium ion batteries. Journal of Power Sources 2009;189(1):101–7.
[20] Panwar N, Kaushik S, Kothari S. Role of renewable energy sources in environmental protection: a review. Renewable and Sustainable Energy Reviews 2011;15(3):1513–24.
[21] Nelson RF. Power requirements for batteries in hybrid electric vehicles. Journal of Power Sources 2000;91(1):2–26.
[22] Burke A. Ultra capacitor technologies and application in hybrid and electric vehicles. International Journal of Energy Research 2010;34(2):133–51.
[23] Saito Y. Thermal behaviors of lithium-ion batteries during high-rate pulse cycling. Journal of Power Sources 2005;146(1–2):770–4.
[24] Yu S, Jung D. Thermal management strategy for a proton exchange membrane fuel cell system with a large active cell area. Renewable Energy 2008;33:2540–8.
[25] Matamoros L, Bruggemann D. Simulation of the water and heat management in proton exchange membrane fuel cells. Journal of Power Sources 2006;161(1):203–13.
[26] Bao C, Ouyang MG, Yi BL. Analysis of the water and thermal management in proton exchange membrane fuel cell systems. International Journal of Hydrogen Energy 2006;31(8):1040–57.
[27] Zong Y, Zhou B, Sobiesiak A. Water and thermal management in a single PEM fuel cell with non-uniform stack temperature. Journal of Power Sources 2006;161(1):143–59.
[28] Yu XC, Zhou B, Sobiesiak A. Water and thermal management for Ballard PEM fuel cell stack. Journal of Power Sources 2005;147(1–2):184–95.
[29] Sung MK, Mudawar I. Single-phase hybrid micro-channel/micro-jet impingement cooling. International Journal of Heat and Mass Transfer 2008;51:4342–52.
[30] Parida PR, Ekkad SV, Khai N. Impingement-based high performance cooling configurations for automotive power converters. International Journal of Heat and Mass Transfer 2012;55:834–47.
[31] Cheong S, Kim T, Kim D. Analysis of water and thermal management with coolant operating conditions for a proton exchange membrane fuel cell. Current Applied Physics 2010;10:22–5.
[32] Dumercy L, Glises R, Louahlia GH, Kauffmann JM. Thermal management of a PEMFC stack by 3D nodal modeling. Journal of Power Sources 2006;156(1):78–84.
[33] Rao ZH, Wang SF. A review of power battery thermal energy management. Renewable and Sustainable Energy Reviews 2011;15:4554–71.
[34] Rami S, Kizilel R, Selman JR, Al-Hallaj S. Active (air-cooled) vs. passive (phase change material) thermal management of high power lithium-ion packs: limitation of temperature rise and uniformity of temperature distribution. Journal of Power Sources 2008;182:630–8.
[35] Jang JC, Rhi SH. Battery thermal management system of future electric vehicles with loop thermosyphon. In: Proceedings of the US–Korea conference on science, technology, and entrepreneurship (UKC). 2010.
[36] Pendergast DR, DeMauro EP, Fletcher M, Stimson E, Mollendorf JC. A rechargeable lithium-ion battery module for underwater use. Journal of Power Sources 2011;196(2):793–800.
[37] Zhang YP, Yu XL, Feng QK, Zhang RT. Thermal performance study of integrated cold plate with power module. Applied Thermal Engineering 2009;29:3568–73.
[38] Mallette M, Venkataraman G. Financial incentives to encourage demand response participation by plug-in hybrid electric vehicle owners. In: Energy conversion congress and exposition (ECCE); 2010. p. 4278–84.
[39] Mills A, Hallaj SA. Simulation of passive thermal management system for lithium-ion battery packs. Journal of Power Sources 2005;141(2):307–15.
[40] Kizilel R, Lateef A, Sabbah R, Farid MM, Selman JR, Al-Hallaj S. Passive control of temperature excursion and uniformity in high-energy Li-ion battery packs at high current and ambient temperature. Journal of Power Sources 2008;183(1):370–5.
[41] Rao ZH, Zhang GQ. Thermal properties of paraffin wax-based composites containing graphite. Energy Sources Part A–Recovery Utilization and Environmental Effects 2011;33(7):587–93.
[42] Otmar B, Guenter G. Systems for hybrid cars. Journal of Power Sources 2004;127:8–15.
[43] Khateeb SA, Amiruddin S, Farid M. Thermal management of Li-ion battery with phase change material for electric scooters: experimental validation. Journal of Power Sources 2005;142:345–52.
[44] Gadalla MA, Ratlamwala T, Dincer I. Energy and energy analyses of an integrated fuel cell and absorption cooling system. International Journal of Energy 2010;7(6):731–54.
[45] Takaki A, Toyoaki N, Hideaki H. Development of a high-power battery cooling system for series HEVs. Belgium, Brussels: EVS-15; 1998.
[46] Osamu W. Battery cooling structure. Kanagawa: Tokyo R&D Co; 10 (US: 06613472).
[47] Pan HB, Zhao JH, Feng XZ, Cao GY, Hu JW, Ge JS. Use of simulation technology on the construction design of nickel hydride metal piles. Chinese Journal of Mechanical Engineering 2005;41(12):58–61.
[48] Fu ZY, Lin CT, Chen QS. Key technologies of thermal management system for EV battery packs. Journal of Highway and Transportation Research and Development 2005;22(3):119–23.
[49] Zhu XT. Study in wind cooling system for RAV-4 EV packs. Nanjing, China: Nanjing: University of Aeronautics and Astronautics; 2007.
[50] Liu ZJ, Lin GF, Qin DT, Hu MH, Lin XY. A study on the temperature field of Lithium-ion battery pack in an electric vehicle and its structural optimization. Automotive Engineering 2012;34(1):80–4.
[51] Javani N, Dincer I, Naterer GF. Thermodynamic analysis of waste heat recovery for cooling systems in hybrid and electric vehicles. Energy 2012;46:109–16.
[52] Zhang YJ, Xie JM, Ouyang MG. The arrangement mode of battery pack cooling mechanism. Tsinghua University; 9(CN: 1401511A).
[53] Li GC. The heat dissipation device of power battery pack. 10(CN: 2660686Y).
[54] Xu XM, Zhao YQ. Research on wind cooling disperse heat of micro electric vehicle power cabin. Journal of Aerospace Power 2012;27(7):1532–6.
[55] Xu XM, He R. Analysis of heat dissipation by natural wind in power cabin of electric vehicle at high speed. Journal of Southeast University (Natural Science Edition) 2013;43(3):520–4.
[56] Xu XM, Zhao YQ. Influence of different double-outlet mode of wind on the electric vehicle natural wind cooling performance. Journal of Harbin Institute of Technology 2013;45(5):70–4.
[57] Xu XM, He R. Research on the wind cooling heat dissipation performance of electric vehicle. ACTA Armamentaria 2013;34(6):657–63.
[58] Xu XM, Zhao YQ. Research on thermal flow field synergy and heat dissipation performance of electric vehicle cooling system. Journal of Mechanical Engineering 2013;49(2):102–8.
[59] Xu XM, He R. Research on the heat dissipation performance of battery pack based on forced air cooling. Journal of Power Sources 2013;240:33–41.
[60] Xu XM, Zhao YQ. Research on battery module thermal characteristics based on double inlet and outlet flow path liquid-cooled system. China Mechanical Engineering 2013;24(3):313–6.
[61] Pesaran AA, Vlahinos A, Burch SD. Thermal performance of EV and HEV battery modules and packs. In: Proceedings of the 14th international electric vehicle symposium. Orlando, Florida; 1997.
[62] Pesaran AA, Burch SD, Keyser M. An approach for designing thermal management systems for electric and hybrid vehicle battery packs. In: Proceedings of the fourth vehicle thermal management systems conference and exhibition. 1999.
[63] Pesaran AA, Keyser M. Thermal characteristics of selected EV and HEV batteries. In: Proceedings of the IEEE sixteenth annual battery conference on applications and advances. 2001.
[64] Pesaran AA, Kim G, Keyser M. Integration issues of cells into battery packs for plug-in and hybrid electric vehicles. In: Proceedings of the 24th international batteries, hybrid and fuel cell electric vehicle symposium. Stavanger; 2009.
[65] Dang T, Teng JT. Comparisons of the heat transfer and pressure drop of the micro channel and mini channel heat exchangers. Heat Mass Transfer 2011;47:1311–22.
[66] Park Y, Jun S, Kim S, Lee DH. Design optimization of a loop heat pipe to cool a lithium ion battery onboard a military aircraft. Journal of Mechanical Science and Technology 2010;24:609–18.
[67] Kizilel R, Sabbah R, Selman JR, Al-Hallaj S. An alternative cooling system to enhance the safety of Li-ion battery packs. Journal of Power Sources 2009;194:1105–12.
[68] Rao ZH, Wang SF, Wu MC, Lin ZR, Li FH. Experimental investigation on thermal management of electric vehicle battery with heat pipe. Energy Conversion and Management 2013;65:92–7.
[69] Hamut HS, Dincer I, Naterer GF. Energy analysis of a TMS (thermal management system) for range-extended EVs (electric vehicles). Energy 2012;46:117–25.
[70] Li D, Yang K, Chen S, Wu F. Thermal behavior simulation of Ni/MH battery. Chinese Science Bulletin 2009;54:1500–6.
[71] Jeon DH, Baek SM. Thermal modeling of cylindrical lithium ion battery during discharge cycle. Energy Converse Manage 2011;52(8–9):2973–81.
[72] Waag W, Kabitz S, Sauer DU. Experimental investigation of the lithium–ion battery impedance characteristic at various conditions and aging states and its influence on the application. Apply Energy 2013;102:885–97.
[73] Kojima T, Ishizu T, Horiba T, Yoshikawa M. Development of lithium-ion battery for fuel cell hybrid electric vehicle application. Journal of Power Sources 2009;189(1):859–63.
[74] Tang Y, Yuan W, Pan M, Wan ZP. Experimental investigation on the dynamic performance of a hybrid PEM fuel cell/battery system for lightweight electric vehicle application. Applied Energy 2011;88:68–76.

[75] Pesaran AA. Battery thermal models for hybrid vehicle simulations. Journal of Power Sources 2002;110:377–82.
[76] Bernardi D, Pawlikowski E, Newman J. A general energy balance for battery systems. Journal of the Electrochemical Society 1985;132:5–12.
[77] Doyle M, Fuller T, Newman J. Modeling of galvanostatic charge and discharge of the lithium/polymer/insertion cell. Journal of the Electrochemical Society 1993;140:1526–33.
[78] Chen Y, Evans J. Heat transfer phenomena in lithium polymer-electrolyte batteries for electric vehicle application. Journal of the Electrochemical Society 1993;140:1833–8.
[79] Newman J, Tiedemann W. Temperature rise in a battery module with constant heat generation. Journal of the Electrochemical Society 1995;142:1054–7.
[80] Pals C, Newman J. Thermal modeling of the lithium/polymer battery. Journal of the Electrochemical Society 1995;142:3274–81.
[81] Doyle M, Newman J, Gozdz A. Comparison of modeling predictions with experimental data from plastic lithium ion cells. Journal of the Electrochemical Society 1996;143:1890–903.
[82] Thomas K, Newman J. Thermal modeling of porous insertion electrodes. Journal of the Electrochemical Society 2003;150:176–92.
[83] Chen Y, Evans JW. Thermal analysis of lithium polymer electrolyte batteries by a two dimensional model: thermal behavior and design optimization. Electrochimica Acta 1994;39(4):517–26.
[84] Srinivasan V, Wang CY. Analysis of electrochemical and thermal behavior of Li-ion cells. Journal of the Electrochemical Society 2003;150:98–106.
[85] Liaw BY, Bethune KP, Yang YG. Advanced integrated battery testing and simulation. Journal of Power Sources 2002;110(2):330–40.
[86] Maleki H, Shamsuri AK. Thermal analysis and modeling of a notebook computer battery. Journal of Power Sources 2003;115(1):131–6.
[87] Doughty DH, Butler PC, Jungst RG. Lithium battery thermal models. Journal of Power Sources 2002;110(2):357–63.
[88] Harmel J, Ohms D, Guth U, Wiesener K. Investigation of the heat balance of bipolar NiMH-batteries. Journal of Power Sources 2006;155(1):88–93.
[89] Kim GH, Pesaran A, Spotnitz R. A three-dimensional thermal abuse model for lithium-ion cells. Journal of Power Sources 2007;170(2):476–89.
[90] Catherino HA. Complexity in battery systems: thermal runaway in VRLA batteries. Journal of Power Sources 2006;158(2):977–86.
[91] Smith K, Wang CY. Power and thermal characterization of a lithium-ion battery pack for hybrid-electric vehicles. Journal of Power Sources 2006;160(1):662–73.
[92] Guo G, Long B, Cheng B, Zhou SQ, Xu P, Cao BG. Three-dimensional thermal finite element modeling of lithium-ion battery in thermal abuse application. Journal of Power Sources 2010;195:2393–8.
[93] Inui Y, Kobayashi Y, Watanabe Y, Watase Y, Kitamura Y. Simulation of temperature distribution in cylindrical and prismatic lithium ion secondary batteries. Energy Conversion and Management 2007;48(7):2103–9.
[94] Lee DH, Kim US, Shin CB. Modeling of the thermal behavior of an ultra capacitor for a 42-V automotive electrical system. Journal of Power Sources 2008;175(1):664–8.
[95] Chen SC, Wan CC, Wang YY. Thermal analysis of lithium-ion batteries. Journal of Power Sources 2005;140(1):111–24.
[96] Wu MS, Liu KH, Wang YY, Wan CC. Heat dissipation design for lithium-ion batteries. Journal of Power Sources 2002;109(1):160–6.
[97] Kwon KH, Shin CB, Kang TH, Kim CS. A two-dimensional modeling of a lithium polymer battery. Journal of Power Sources 2006;163:151–7.
[98] Jegadheeswaran S, Pohekar SD. Performance enhancement in latent heat thermal storage system: a review. Renewable and Sustainable Energy Reviews 2009;13(9):2225–44.
[99] Cai L, White RE. An efficient electrochemical-thermal model for a lithium-ion cell by using the proper orthogonal decomposition method. Journal of the Electrochemical Society 2010;157:1188–95.
[100] Kim US, Shin CB, Kim C. Modeling for the scale-up of a lithium-ion polymer battery. Journal of Power Sources 2009;189:841–6.
[101] Kuperman A, Aharon I. Battery-ultra capacitor hybrids for pulsed current loads: a review. Renewable and Sustainable Energy Reviews 2011;15:981–92.
[102] Nelson P, Dees D, Amin K, Henriksen G. Modeling thermal management of lithium-ion PNGV batteries. Journal of Power Sources 2002;110(2):349–56.
[103] Pesaran AA, Burch SD, Keyser M. An approach for designing thermal management systems for electric and hybrid vehicle battery packs. In: Proceedings of the 4th vehicle thermal management systems. London: UK: Professional Engineering Publishing LTD.; 1999. p. 331–46.
[104] Lin CT. Research on the modeling and management of nickel metal hydride battery packs for electric vehicles. Beijing: Tsinghua University; 2006 [in Chinese].
[105] Chen LT, Xu SC, Chang GF. A study on the flow field characteristics of HEV battery thermal management system. Automotive Engineering 2009;31(3):224–7.
[106] Mahamud R, Park C. Reciprocating air flow for Li-ion battery thermal management to improve temperature uniformity. Journal of Power Sources 2011;196(13):5685–96.
[107] Liang JH. Research on the heat dissipation of pure EV's battery pack. Beijing: Tsinghua University; 2011 [in Chinese].
[108] Zolot M, Pesaran AA, Mihalic M. Thermal evaluation of Toyota Prius battery pack. Hyatt Crystal City: Future Car Congress 2002.
[109] Lou Y. Nickel-metal hydride battery cooling system research for hybrid electric vehicle. Shanghai: Shanghai Jiao Tong University; 2007 [in Chinese].
[110] Fang W, Kwon OJ, Wang C. Electrochemical-thermal modeling of automotive Li-ion batteries and experimental validation using a three electrode cell. International Journal of Energy Research 2010;34:107–15.
[111] Abraham DP, Dees DW, Christophersen J, Ho C, Jansen AN. Performance of high-power lithium-ion cells under pulse discharge and charge conditions. International Journal of Energy Research 2010;34:190–203.
[112] Lux SF, Schmuck M, Jeong S, Passerini S, Winter M. Li-ion anodes in air-stable and hydrophobic ionic liquid-based electrolyte for safer and greener batteries. International Journal of Energy Research 2010;34:97–106.
[113] Yang XG, Taenaka B, Miller T, Snyder K. Modeling validation of key life test for hybrid electric vehicle batteries. International Journal of Energy Research 2010;34:171–81.
[114] Smith K, Kim G, Darcy E, Pesaran A. Thermal/electrical modeling for abuse-tolerant design of lithium ion modules. International Journal of Energy Research 2010;34:204–15.
[115] Weinert JX, Burke AF, Wei XZ. Lead–acid and lithium-ion batteries for the Chinese electric bike market and implications on future technology advancement. Journal of Power Sources 2007;172(2):938–45.
[116] Pesaran AA. Battery thermal management in EVs and HEV: issues and solutions. In: Proceedings of the advanced automotive battery conference. Las Vegas, Nevada; 2001.
[117] Dallinger D, Wietschel M. Grid integration of intermittent renewable energy sources using price-responsive plug-in electric vehicles. Renewable and Sustainable Energy Reviews 2012;16:3370–82.
[118] Ramasamy RP, White RE, Popov BN. Calendar life performance of pouch lithium-ion cells. Journal of Power Sources 2005;141(2):298–306.
[119] Zhang Q, White RE. Calendar life study of Li-ion pouch cells. Journal of Power Sources 2008;179(2):785–92.
[120] Takei K, Kumai K, Kobayashi Y, Miyashiro H, Terada N, Iwahori T. Cycle life estimation of lithium secondary battery by extrapolation method and accelerated aging test. Journal of Power Sources 2001;97(8):697–701.
[121] Huang KL, Wang ZX, Liu SQ. The principles and key technologies of lithium-ion battery. Beijing: Chemical Industry Press; 2007 [in Chinese].
[122] Choi SS, Lim HS. Factors that affect cycle-life and possible degradation mechanisms of a Li-ion cell based on $LiCoO_2$. Journal of Power Sources 2002;111(1):130–6.
[123] Pesaran AA, Swan D, Olson J. Thermal analysis and performance of a battery pack for a hybrid electric vehicle. In: Proceedings of the electric vehicle symposium. Brussels, Belgium; 2002.
[124] Hallaj SA, Selman JR. Thermal modeling of secondary lithium batteries for electric vehicle/hybrid electric vehicle applications. Journal of Power Sources 2002;110:341–8.
[125] Cosley MR, Garcia MP. Battery thermal management system. Chicago, USA: INTELEC; 2004.
[126] Ramadass P, Haran B, White R, Popo VB. Capacity fade of sony 18650 cells cycled at elevated temperatures part II. Capacity fade analysis. Journal of Power Sources 2002;112(2):614–20.
[127] Li H, Su J. Cycle-life prediction model studies of lithium-ion batteries. Chinese Journal of Power Sources 2008;32(4):242–6.
[128] Hong JS, Maleki H, Redey L. Electrochemical–calorimetric studies of lithium-ion cells. Journal of the Electrochemical Society 1998;145:1489–501.
[129] Sato N. Thermal behavior analysis of lithium-ion batteries for electric and hybrid vehicles. Journal of Power Sources 2001;99(1–2):70–7.